International Journal of Impact Engineering 117 (2018) 48–62

Contents lists available at ScienceDirect

International Journal of Impact Engineering

journal homepage: www.elsevier.com/locate/ijimpeng

Performance-based design procedure of a novel friction-based cladding connection for blast mitigation

Liang Cao[a,*], Sijia Lu[a], Simon Laflamme[a,b], Spencer Quiel[c], James Ricles[c], Douglas Taylor[d]

[a] Department of Civil, Construction, and Environmental Engineering, Iowa State University, Ames, IA 50011, USA
[b] Department of Electrical and Computer Engineering, Iowa State University, Ames, IA 50011, USA
[c] Department of Civil and Environmental Engineering, Lehigh University, Bethlehem, PA 18015, U.S.A
[d] Taylor Devices, North Tonawanda, NY 14120, U.S.A

ARTICLE INFO

Keywords:
Semi-active damping
High performance control systems
Variable friction
Cladding
Structural control
Blast mitigation
Performance-based design

ABSTRACT

Cladding systems are conventionally designed to provide buildings with environmental protection against wind, temperature, humidity, moisture, etc. Recently, researchers have proposed to leverage these systems to provide additional protection against manmade (e.g., blast) and natural (e.g., earthquakes, hurricanes) hazards. This can be achieved, for example, by redesigning the connection between the cladding and the structural system to provide energy dissipation via friction. While promising, the use of flexible cladding connection has only been considered for singular hazards. In this study, the authors propose a novel semi-active damping system to connect the cladding to the structure via a variable friction mechanism. By varying the normal force applied on friction plates through a system of adjustable toggles, it is possible to mitigate vibrations over a wide frequency range, therefore enabling mitigation of different types of hazards (i.e. to achieve multi-hazard resistance). In its passive in-situ mode, the device is designed to provide very high stiffness and friction resistance to mitigate the effects of blast.

The objective of this paper is to enable a holistic integration of said device within the structural design process by developing a performance-based design procedure. The study will focus on the passive in-situ mode of the device, which will provide a stepping stone for the development of performance-based design procedures for its semi-active (i.e. actuated) capabilities. The proposed performance-based design procedure consists of the following: 1) determine the design performance criteria, including the blast properties and allowable connection gap between the cladding and structure; 2) select design properties for the cladding connection, including stiffness and damping; and 3) design a rubber impact bumper located between the structure and the cladding in order to mitigate slamming of the cladding into the structure for very high blast loads.

1. Introduction

Civil infrastructures, including buildings and energy, lifeline, communication, and transportation systems, provide significant services and benefits to our communities. These systems need to be designed, constructed, and maintained to sufficiently resist the effects of service and extreme loads so that their continuous daily operability and public safety can be sustained. In particular, modern construction techniques and materials enable the construction of lighter and more flexible structures - as an example, increasing wind-induced vibrations which may create discomfort to occupants and result in frequent inoperability of that structure. Also, recent extreme events (e.g., earthquakes, hurricanes, tornadoes, storm surges, accidental and intentional blasts) have illustrated the vulnerabilities of buildings and transportation infrastructures to sudden losses in functionality.

A solution to increase structural performance to extreme loads in particular is a performance-based design (PBD) approach [1]. For dynamic loads, the strategy is to appropriately size structural stiffness, damping, and inertia such that the resulting response meets a prescribed performance level. For wind and seismic loads, the targeted response can often be achieved via the implementation of supplemental damping systems [2]. In cases when multiple excitation inputs are considered individually or as a combination (i.e. multi-hazard excitations), a PBD approach becomes difficult to implement with a passive supplemental damping strategy.

It is possible to leverage cladding systems for mitigation of different hazards. Cladding serves both as the point of application of externally applied lateral loads such as wind and blast as well as a contributor of

* Corresponding author.
E-mail address: lic418@lehigh.edu (L. Cao).

https://doi.org/10.1016/j.ijimpeng.2018.03.003
Received 5 March 2017; Received in revised form 15 November 2017; Accepted 10 March 2018
Available online 12 March 2018

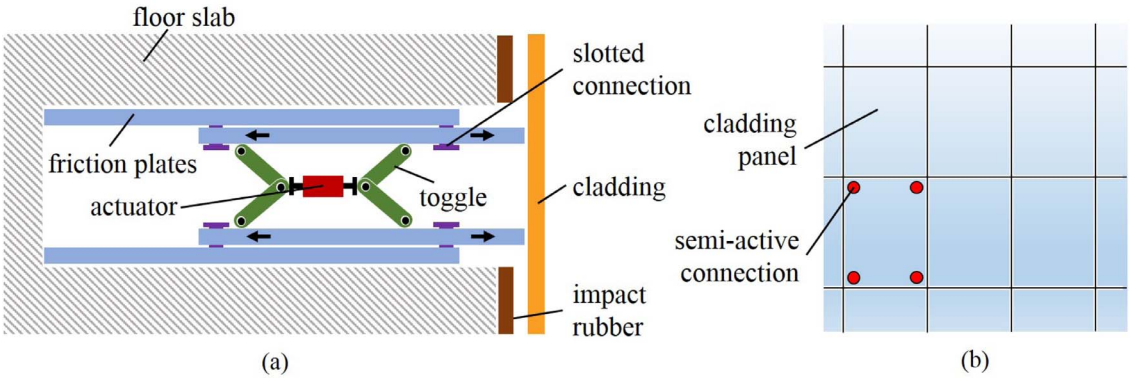

Fig. 1. Semi-active device integrated in (a) floor slab (top view); and (b) building façade (elevation view).

inertial force via the excitation of its mass due to seismic or wind-induced vibrations. As designed in current practice, the cladding is mounted to the structure via tie-back connections, commonly comprised of angles bolted to embeds in the floor slab diaphragm and cladding panel. Since conventional connections are very stiff, the cladding will typically not be an active participant in resisting seismic and wind loads. The cladding is typically designed to suffer some permanent deformations and damage yet not experience blowout when subjected to blast loading, but the cladding elements may transfer significant reactions to the structure, thus requiring the cladding-to-structure connections to be strengthened. Rigid support of the cladding will not provide energy dissipation for intense but short-duration blast loads, thereby ensuring that both the cladding and the building itself will undergo a maximum response to the load.

Passive cladding connections have been previously proposed for dissipating energy from earthquake excitation. In these systems, the cladding is utilized as a mass damper which helps mitigate inertial loading due to seismic vibration rather than merely contributing to those loads as an added mass source. Early work by others [3,4] examined ductile connections and demonstrated their ability to reduce interstory floor drifts. More recently Maneetes and Mermari [5] proposed a passive friction damper that is designed to slip when subjected to moderate to high intensity earthquakes. Baird et al. [6] proposed a U-shaped flexural plate connection to dissipate earthquake energy. Previous research has also considered on passive energy dissipation for blast loads. A significant amount of early research has focused on the use of sacrificial systems composed of foam-based materials that are placed in locations that experience bearing during a blast event [7,8]. Though effective under certain blast conditions, these materials offer little potential for resisting multiple hazards since they are not capable of dissipating energy for lower frequency loading. Few studies have been performed to explore the use of damping devices rather than sacrificial crushing materials or devices for blast applications. Among these studies are those by Amadio and Bedon [9] [10], who have recently investigated the use of viscoelastic dampers at the lateral connection of blast-resistant curtain wall systems to the structure. The results of these studies have shown that the viscoelastic dampers provide significant reductions in the peak response of the curtain wall systems that were considered [9]. These reductions enable both a lighter design of the curtain wall to meet the same level of blast resistance and a reduction of the reactions transmitted to the structural system.

All of these examples of energy dissipation connectors are passive systems, whose mitigation capabilities are limited over a relatively narrow performance bandwidth [11–13], and are therefore limited to mitigating single specific types of hazards. Alternatively, semi-active, hybrid, and active structural control solutions can be used to tailor the performance of connection devices to a wider spectrum of loading demands and frequencies. These high-performance control systems (HPCSs) can perform over a wide excitation bandwidth and are ideal for multi-hazard applications. Several examples of devices enabling HPCS are provided in the referenced literature[14–19].

In this paper, the authors propose a novel semi-active connector for cladding systems to provide multi-hazard mitigation. The device is based on a variable friction mechanism which is placed at the lateral connection interface between the cladding and the floor slab diaphragm. Semi-actively controlled friction has gained popularity due to its high energy dissipation and low power requirement. The friction force is generated by contact plates with specifically selected materials and controlled by an actuator, which can apply a varying normal force to the plates via adjustable toggles. Typical actuator types used in generating the normal force include pneumatic [20,21], hydraulic [22], electro-magnetic [23,24], electro-mechanical [25] and piezoelectric [26–29] devices. Examples of large-scale variable friction devices include 25 kN [30,31] and 45 kN [32] capacity systems.

The friction plates can be unlocked and actuated via the semi-acive control algorithm to provide variable friction force for wind and earthquake hazard mitigation. However, the proposed semi-active connection is designed to be in a passive in-situ configuration (at which the actuator is locked and the resulting friction is constant) during daily operations. This configuration is engineered for blast resistance because blast loading, whether from an accidental or intentional explosion, is difficult to predict and occurs too suddenly for a semi-active control algorithm to respond. Given the novelty of the semi-active connection, PBD procedures need to be developed to facilitate the holistic integration of these devices into the structural design. This paper focuses on the design of the device in its passive in-situ configuration to maintain daily operations and withstand unpredictable blast events.

2. Semi-Active connection

The proposed connection is a novel semi-active friction device which provides a lateral connection between the cladding and the floor diaphragm of the buildings structural system. The device, schematized in Fig. 1(a), consists of sliding friction plates subjected to a normal force produced by an actuator applied via a toggle system. The device is inset into prefabricated box-out in the floor slab in order to provide a high degree of mechanical restraint. The device is set into the box-out, which consists of steel plates that are anchored into the slab via metal studs, with its friction plates oriented vertically (thus pushing outward against the high stiffness provided by the slab). The inner plates of the device extend outward to connect to the interior face of the cladding. A rubber impact bumper is integrated between the interface of the cladding and the slab edge (Fig. 1(a)) in order to mitigate slamming of the cladding into the structure. The device is designed to provide equivalent damping due to friction hysteresis based on a decentralized scheme, where each cladding panel (Fig. 1(b)) is damped individually between each floor. Other configurations can be used to accommodate construction preferences, cladding types, and load demands. For example,

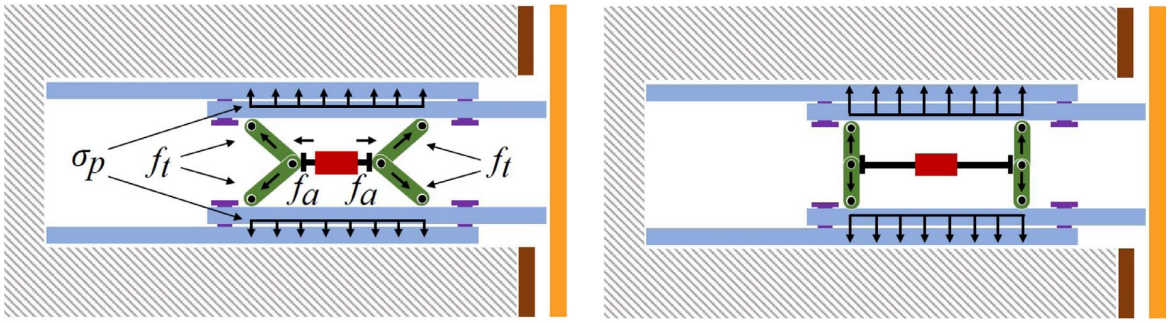

Fig. 2. Schematic of the semi-active device mechanism: (a) unlocked mode; and (b) locked mode.

only the bottom connections to the cladding could be semi-active, while the top connections could be conventional gravity hanger connections.

The force diagram of the proposed connection is illustrated in Fig. 2. The actuator generates a controllable force f_a to push or pull the toggles. Changes in the toggles' geometry provide the variation in the friction force f_t, resulting in a variable normal pressure σ_p on the friction plates. The device can be used in three different damping configurations:

1. Toggles are locked for daily operations (Fig. 2(a)). Both toggles are pushed vertically and provide the maximum normal pressure σ_p on the friction plates, thus locking of the device in a high friction mode. This is the passive in-situ mode, because no power is required to maintain the toggles in the locked position. The actuator remains in its position and acts as a stiff element. This high state of friction is sufficient to avoid slippage of the connection during low-to-moderate loading, during which the cladding system performs similar to any conventional cladding system with "rigid" connections to the structure. The passive mode will also be designed for blast load mitigation such that the blast-induced reactions from the cladding panel will be higher than the connections static friction, resulting in slippage of the connection and energy dissipation. No feedback control is required during blast.
2. Toggles are unlocked and allow variable friction via the actuator. The normal pressure σ_p is varied by the actuator force f_a and the device behaves as a semi-active friction damper. This particular configuration can be used to control interstory drift to limit damage to cladding (e.g. under extreme wind or seismic events).
3. Toggles are disconnected. The friction plates are fully disengaged and the resistance provided by the connection is minimal, resulting in near-zero axial force f_t and normal pressure σ_p. This configuration is also passive, as no power input is necessary once the toggles are retracted. This configuration can be used to limit acceleration transfer to floors as well as to reset the connections to their initial state following their response to an extreme event.

In what follows, PBD procedures are developed for configuration 1 (toggles locked for daily operations). While the proposed mitigation device is very specific, such PBD procedures could be modified and/or applied to any passive device based on friction and impact rubber mechanisms used in dissipating blast loads. Representative models of the device performance based on current prototypes will be used to demonstrate the PBD procedure. Note that the fabrication and characterization of a prototype is part of a current investigation and is out-of-the-scope of this paper. The re-positioning of the device and cladding is also left to future work; because a manual reset could be impractical, one would need to engineer a mechanism enabling automatic reset, termed self-centering mechanism.

3. Methodology

The dynamics of the structure-cladding interaction under blast loading is nonlinear given the presence of a friction element and an impact bumper (nonlinear stiffness) in combination with the high peak and rapid time decay of a blast load. Some simplifications are made in order to facilitate the derivation of analytical solutions, which will be used to estimate transfer functions that utilize PBD. The analytical solutions will be derived for the first half-cycle displacement response of the cladding following a blast load, which corresponds to the maximum displacement of the cladding and highest possible impact force on the building. This section discusses the simplified models used for the derivation of these solutions. These solutions are then compared with computational models to verify the applicability of the analytical simplifications.

3.1. Structure-cladding model

The structure-cladding interaction is studied both in a single-degree-of-freedom (SDOF) and a two degree-of-freedom (2DOF) configuration. The SDOF configuration is utilized to derive analytical solutions for PBD procedures. In this model, the structure is fixed based on the assumption that the dynamics of the structure itself can be negligible during the first half-cycle of the claddings displacement. This assumption is often used in the simulation of cladding components when subjected to short duration blast loads [33–36]. Fig. 3(a) shows the SDOF representation of the cladding and its connection. The cladding of mass m_c is connected to the structure via a stiffness element k_c and a viscous element c_c, and a friction element f_c. The friction element f_c represent the friction force from proposed semi-active device and k_c and c_c stand for the total stiffness and damping properties of cladding system including the gravity connection and non-friction components of proposed device. An impact rubber of length l_r is installed at a distance l_c from the structure. The rubber is modeled as a nonlinear stiffness element k_r and viscous damping element c_r . The blast load is represented by a time series $p(t)$. The 2DOF configuration, represented in Fig. 3(b), is used for verifying the design methodology over a more realistic dynamics. In this representation, the cladding is connected to the structure of mass m_s, connected to its based by a stiffness element k_s and a viscous element c_s.

3.2. Blast load model

A typical blast pressure wave in shown in Fig. 4(a) [37]. At the beginning of the explosion, the air pressure builds up very rapidly to the peak reflected pressure value σ_{max}. The pressure decays over time t_d (positive phase duration) and drops to the negative pressure σ_{min} before dissipating over time t_n, (negative phase duration) for a total blast time duration $t_{blast} = t_d + t_n$. The positive phase ($t < t_d$) can be modeled using the general descending pulse model proposed by Li et al. [38] and

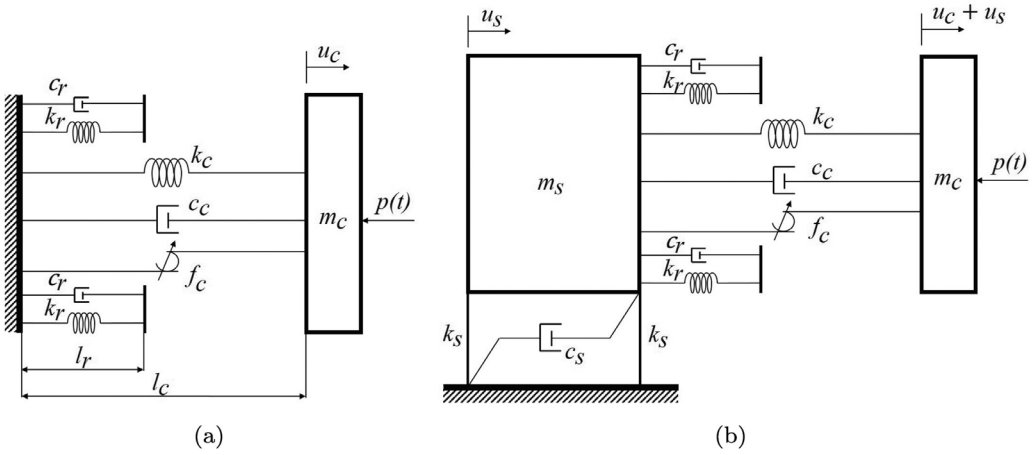

Fig. 3. (a) SDOF representation; and (b) 2DOF representation.

the negative phase can be modeled by a bilinear function [39].

In this study, the blast load is simplified using a linear approximation for the positive phase and neglecting the minimum pressure ($\sigma_{min} \approx 0$ and $t_{blast} = t_d$). This idealized blast model is shown in Fig. 4(b) in accordance with the current state of practice criteria documents for blast resistance [40]. The blast load $p(t)$ is taken as

$$p(t) = \begin{cases} F_m\left(1 - \frac{t}{t_{blast}}\right) & \text{if} \quad 0 < t < t_{blast} \\ 0 & \text{if} \quad t > t_{blast} \end{cases} \tag{1}$$

where $F_m = A_c \sigma_{max}$ is the peak blast force, and A_c is the area of the cladding. The blast impulse I is taken as

$$I = \int_0^{t_{blast}} p(t)dt = \frac{1}{2} F_m t_{blast} \tag{2}$$

For this study, it is assumed that the cladding will not fail under σ_{max}, with $\sigma_{max} \leq \sigma_{cap}$ where σ_{cap} is the ultimate resistance of the cladding to avoid blowout failure. For example, government design criteria in the United States require fenestration to resist pressures in the range 27.6–276 kPa (4–40 psi) depending on the criteria document [41].

The plastic energy absorption of cladding panels has been previously studied. Ye and Ma [42] proposed a load-cladding-structure model to investigate the mitigation performance of a foam cladding structure against blast loads. The study demonstrated that the proposed foam cladding could absorb up to 60% of the blast energy. Li et al. [43] conducted a finite element analysis to investigate the response of a six-story concrete structure with exterior reinforced concrete (RC) cladding panels subjected to far-field blast loads. Results showed that RC exterior cladding panels converted nearly 40% of the blast energy into the plastic strain energy. Recently, Zhao et al. [44] proposed a foamed cement-based sacrificial cladding and investigated its blast mitigation effect with varied cladding thickness by finite element analysis. The study demonstrated that the peak stress of structure could be reduced by 10% and 20% using 6 cm and 8 cm-thickness foamed cladding, respectively.

The focus of this study is on the transfer of blast-induced reactions from the cladding to the structure, not the blast resistant design of the cladding itself. The nonlinear response of the individual cladding panels to the blast load will be incorporated in future iterations of this procedure. The current approach is conservative with regard to its intended focus because it assumes that all blast-induced forces are transferred through the cladding-to-structure connections with no potential energy absorption or dissipation provided by the plastic response or partial damage (such as cracking or shallow spalling) of the cladding. The nonlinear cladding response is also commonly neglected in current practice when calculating the maximum base shear experienced by buildings under blast loading [45,46].

3.3. Impact rubber model

Several models have been developed for rubber impact bumpers, such as the linear impact spring, linear viscoelastic impact [47], the Hertz model with nonlinear spring [48] , and the Hertz model with nonlinear damping models [49–51]. Here, the model presented by Polycarpou et al. [49] for a structural impact mitigation bumpers is selected. In this model, the resistive force of the impact rubber F_r is written:

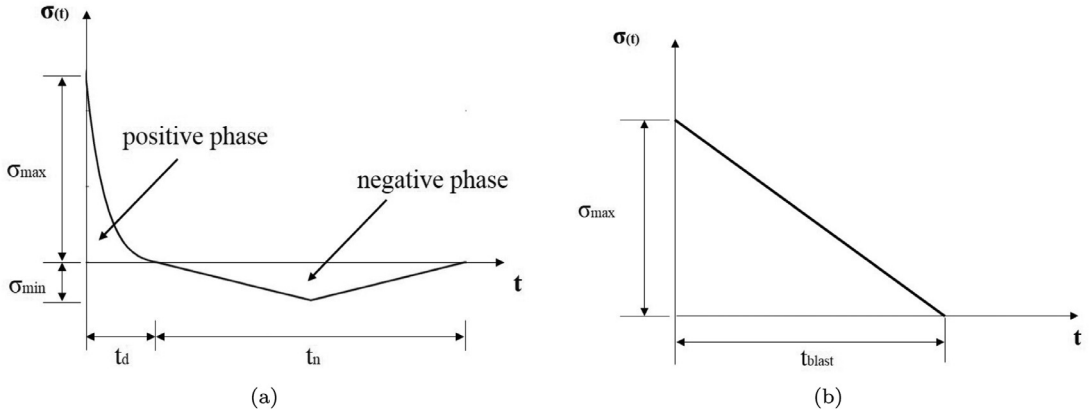

Fig. 4. Time history curve for air blast wave pressure : (a) typical time history ; and (b) idealized time history.

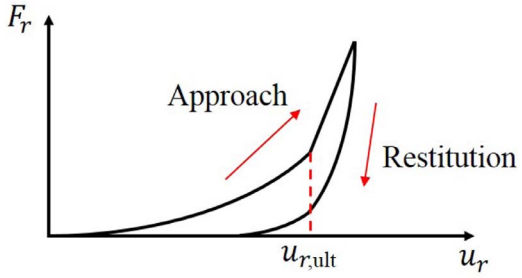

Fig. 5. Nonlinear rubber impact hysteresis.

$$F_r = \begin{cases} k_r u_r^n & \text{for } u_r < u_{r,\text{ult}} \quad \dot{u}_r > 0 \\ k_r u_{r,\text{ult}}^n + k_{r,y}(u_r - u_{r,\text{ult}}) & \text{for } u_r > u_{r,\text{ult}} \quad \dot{u}_r > 0 \\ k_r u_r^n (1 + c_r \dot{u}_r) & \text{for } \dot{u}_r < 0 \end{cases} \tag{3}$$

where u_r and $u_{r,\text{ ult}}$ are the displacement and the ultimate compression capacity of the impact rubber, respectively; k_r and $k_{r,\text{ y}}$ are the impact stiffness and the post-yield stiffness of the impact rubber, respectively; $n > 1$ is the impact exponent; and c_r is the impact rubber damping coefficient. The impact rubber stiffness k_r is taken as

$$k_r = \beta \frac{A_r k_r'}{l_r^n} \tag{4}$$

where β is a strain rate-dependent coefficient, A_r is the contact area of the impact rubber, and k_r' is the stiffness of the material. The value $\frac{A_r k_r'}{l_r^n}$ represents the static stiffness of the impact rubber. Reference [49] provides a semi-empirical equation to determine c_r

$$c_r = \frac{3(1 - \text{COR}^2)}{2 \cdot \text{COR} \cdot \dot{u}_{\text{rubber}}} \tag{5}$$

where $\dot{u}_{\text{rubber}}$ is impact velocity, and COR is the coefficient of restitution. Example values for all parameters can be found in Reference [49]. Fig. 5 shows the typical force-displacement (F_r - u_r) loop for the impact rubber based on that model.

4. Performance-Based design procedure

The proposed 3-step PBD procedure for the semi-active cladding connection system exposed to a blast load is illustrated in Fig. 6. Step 1 determines the design performance criteria, which include the maximum blast design pressure $\sigma_{\max}$ along with its period t_{blast} and the spacing l_c between the cladding and structure. The peak pressure and duration of blast can be obtained from the literature [40] based on the explosive charge mass and the standoff distance. Step 2 consists of designing the dynamic parameters of the cladding system, including m_c, c_c, k_c, and F_c, and obtaining the maximum displacement of the cladding $u_{c,\text{ max}}$ based on transfer function H_1 to be compared with the performance parameter l_c from Step 1. If $u_{c,\text{ max}} \leq l_c$ the cladding will not collide with the structure, and the design of the impact rubber can be based on fail-safe requirements if the cladding will also not collide with the rubber ($u_{c,\max} \leq (l_c - l_r)$). Otherwise, if the cladding is to collide with any element, Step 3 is then used to design the impact rubber design. The rubber thickness l_r will be designed in order to dissipate energy with a prescribed maximum compression of $u_{r,\text{ max}}$, obtained through transfer functions H_2 and H_3. If $u_{r,\text{ max}} \leq l_c$ is satisfied, then the design procedure is finished. Otherwise, three design options could be considered: (1) change the allowable spacing l_c, (2) change the dynamic parameters of the cladding system, or (3) iterate on the rubber thickness l_r. The proposed PBD procedure is conducted using an SDOF system, and design parameter values will be selected from analytical solutions. It is assumed that the peak dynamic response of cladding panel to blast will occur at the first quarter cycle, and the dynamics of the structure can be assumed negligible during the maximum cladding response (i.e. there will be a delay between the maximum response of the cladding and that of the building due to high-speed load transfer). Although numerical solutions are more exact, the analytical solution would allow designers to quickly select design parameters, therefore enabling a holistic integration of the device within the structural design stage. Each step of the procedure is described in detail below.

4.1. Step 1 : Performance criteria

The first step is to establish parameters that will define the performance requirements of the cladding system. These include the selection of the design blast load, and the allowable gap distance between the cladding and structure l_c.

4.1.1. Design blast pressure

The design blast pressure can be selected based on three parameters: the explosive material, the explosive charge weight W, and the standoff distance between the blast source and the target R. Most severe intentional blast threats are vehicle-borne, and the mass of the explosive charge can be estimated based on quantities of explosive that can be stored in various vehicles. Reference [52] provides estimated quantities of common explosives based on vehicle types. To obtain the resulting blast pressure, the charge mass from different explosive material is represented as an equivalent mass of TNT [53].

The standoff distance R can be based on several factors, including site security, roadway access, and topography. The minimum standoff distance for inhabited buildings of conventional construction can be directly obtained from Section 2.3.2.2.1 of ASCE/SEI 59-11 [54]. Based on the assumption that the explosive consists of TNT, the following equation can be used to relate W and R to the peak incident overpressure σ_{so} [55]:

$$\sigma_{\text{so}} = \frac{1772}{Z^3} - \frac{114}{Z^2} + \frac{108}{Z} \tag{6}$$

where σ_{so} is in kPa, W is in kg, and $Z = \frac{R}{W^{\frac{1}{3}}}$ is the scaled distance with R is in m. The peak reflected pressure $\sigma_{\max}$ is

$$\sigma_{\max} = C_r \sigma_{\text{so}} \tag{7}$$

where C_r is the reflection coefficient defined as [46,56]

$$C_r = 3\left(\frac{\sigma_{\text{so}}}{101}\right)^{\frac{1}{4}} \tag{8}$$

Lastly, the design peak blast force is taken as $F_m = A_c \sigma_{\max}$, and its associated period t_{blast} (in ms) determined from Eq. 9 [56]:

$$t_{\text{blast}} = W^{1/3} 10^{[-2.75 + 0.27 \log(Z)]} \tag{9}$$

4.1.2. Allowable distance cladding-structure

Typically, cladding panels are connected to the structure through hanger supports to resist gravity loads and tieback connections to resist lateral loads. The lateral connections require a minimum spacing $l_{c,\text{ min}}$ between the cladding panel and the structure for their installation, and can be as high as 6 in (15 cm) for prefabricated panels [57]. Allowances for rain drainage, mortar droppings, vapor diffusion, and fire/smoke spread prevention need to be taken into account as well. Free drainage occurs if the airspace is greater than 3/8 in (1 cm) [58]. A minimum of 1 in (2.54 cm) airspace is needed to allow quick drying for the wall, thus impeding bacteria growth. For cast-in-place or site-installed cladding such as brick veneer, a minimum 2 inch airspace is recommended to reduce the possibility that the mortar squeezes out into the air space during brick laying and makes permanent contact with the structure. In this study, it is assumed that the cladding is designed to avoid blowout under blast load; therefore, prefabricated cladding, which is generally more robust for lateral loads, is considered. Preliminary design of the spacing l_c needs to meet the aforementioned requirements with no less than the minimum gap spacing $l_{c,\text{ min}}$.

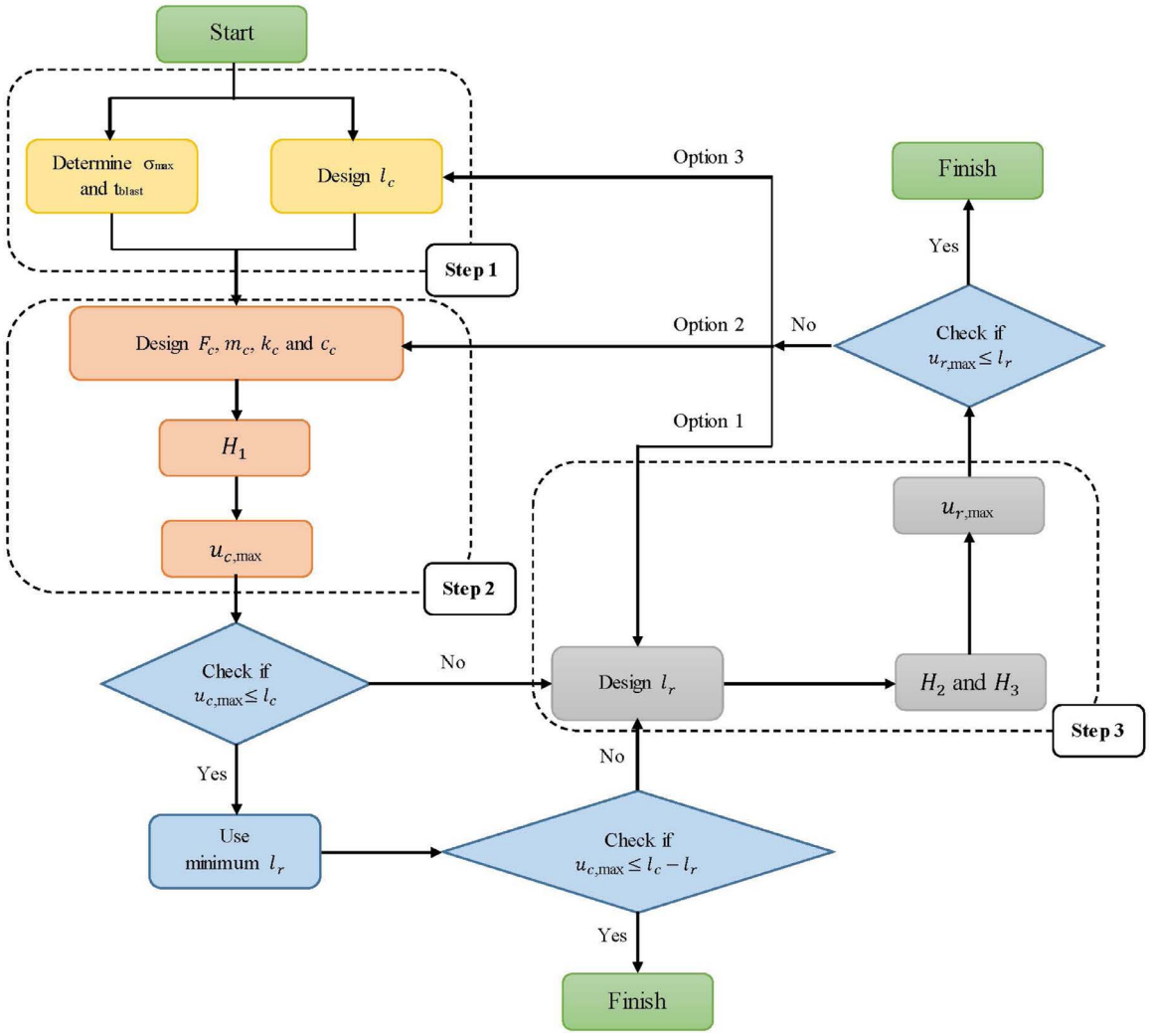

Fig. 6. 3-steps performance based design procedure.

4.2. Step 2 : Dynamic parameters of cladding system

The second step in the design is to select the dynamic parameters of the cladding system, including the friction capacity of the semi-active connection (used in passive mode). The equation of motion of an SDOF representation of the cladding system subjected to a blast load can be written

$$m_c\ddot{u}_c + c_c\dot{u}_c + k_c u_c + F_c = F_m\left(1 - \frac{t}{t_{\text{blast}}}\right) \quad \text{for} \quad 0 \le t \le t_{\text{blast}} \tag{10a}$$

$$m_c\ddot{u}_c + c_c\dot{u}_c + k_c u_c + F_c = 0 \quad \text{for} \quad t \ge t_{\text{blast}} \tag{10b}$$

with the friction force F_c is approximated using the Coulomb model:

$$F_c = f_c \text{sgn}(\dot{u}_c) \tag{11}$$

where f_c is the friction capacity of the cladding connection, and sgn is the sign or signum function:

$$\text{sgn}(\dot{u}_c) = \begin{cases} -1 & \text{if} \quad \dot{u}_c < 0 \\ 0 & \text{if} \quad \dot{u}_c = 0 \\ 1 & \text{if} \quad \dot{u}_c > 0 \end{cases} \tag{12}$$

Because only the first quarter cycle of the response is considered, $F_c = f_c$. Eq. 10 can be used to characterize the dynamics of the cladding system before it collides with the impact rubber. Assuming that the first quarter cycle response time $T/4 \gg t_{\text{blast}}$, Eq. 10(a) is solved to find the initial conditions for $u_c(t_{\text{blast}})$ and $\dot{u}_c(t_{\text{blast}})$ which are needed to solve Eq. 10(b).

The solution of Eq. 10 (a) can be derived by Duhamels integral,

$$u_c(t) = \frac{1}{m\omega_d}\int_0^t \left[F_m\left(1 - \frac{\tau}{t_{\text{blast}}}\right) - f_c\right] e^{-\xi\omega_n(t-\tau)} \sin[\omega_d(t-\tau)]d\tau \tag{13}$$

where ξ, ω_n and ω_d are the damping ratio, natural frequency, and damped frequency of the cladding system, respectively. The final solution after integration by parts is expressed:

$$\begin{aligned} u_c(t) = \; & e^{-\xi\omega_n t}\left[\left(u_0 - \frac{f_c}{k_c}\right)\cos\omega_d t + \frac{\dot{u}_0 + \left(u_0 - \frac{f_c}{k_c}\right)\xi\omega_n}{\omega_d}\sin\omega_d t\right] + \frac{f_c}{k_c} \\ & + \frac{F_m}{k_c}\left[1 - e^{-\xi\omega_n t}\left(\frac{\xi}{\sqrt{1-\xi^2}}\sin\omega_d t + \cos\omega_d t\right)\right] \\ & - \frac{F_m}{k_c t_{\text{blast}}}\left[t - \frac{2\xi}{\omega_n} + \frac{e^{-\xi\omega_n t}}{\omega_n}\left(2\xi\cos\omega_d t + \frac{2\xi^2 - 1}{\sqrt{1-\xi^2}}\sin\omega_d t\right)\right] \end{aligned} \tag{14}$$

and

$$\dot{u}_c(t) = e^{-\xi\omega_n t}\left[\dot{u}_0\cos\omega_d t - \left(\frac{u_0\omega_n - \frac{f_c}{k_c}\omega_n + \xi\dot{u}_0}{\sqrt{1-\xi^2}}\right)\sin\omega_d t\right] + \frac{F_m e^{-\xi\omega_n t}}{k_c\sqrt{1-\xi^2}}\sin\omega_d t - \frac{F_m}{k_c t_{\text{blast}}}\left[1 - e^{-\xi\omega_n t}\left(\cos\omega_d t + \frac{\xi}{\sqrt{1-\xi^2}}\sin\omega_d t\right)\right] \tag{15}$$

where $0 \le t \le t_{\text{blast}}$. The solutions of Eq. 14 at $t = t_{\text{blast}}$ are used as initial condition for Eq. 10(b). Eq. 10(b) can be solved using the summation of the homogenous solution and particular solution:

$$u_c(t) = e^{-\xi\omega_n(t-t_{\text{blast}})}\left[\left(u_c(t_{\text{blast}}) - \frac{f_c}{k_c}\right)\cos\omega_d(t-t_{\text{blast}}) + \frac{\dot{u}_c(t_{\text{blast}}) + \left(u_c(t_{\text{blast}}) - \frac{f_c}{k_c}\right)\xi\omega_n}{\omega_d}\sin\omega_d(t-t_{\text{blast}})\right] + \frac{f_c}{k_c} \tag{16}$$

where $t > t_{\text{blast}}$. Eq. 16 is used to find the maximum displacement, which occurs at time t_1. Taking the derivative of Eq. 16 equal to zero, and the result of t in first cycle can infer to the maximum u_c, $u_{c,\ \max}$.

$$t_1 = \frac{\tan^{-1}\left(\frac{\dot{u}_c(t_{\text{blast}})\sqrt{1-\xi^2}}{\left(u_c(t_{\text{blast}}) - \frac{f_c}{k_c}\right)\omega_n + \xi\dot{u}_c(t_{\text{blast}})}\right)}{\omega_d} + t_{\text{blast}} \tag{17}$$

$$u_{c,\max} = e^{-\xi\omega_n(t_1-t_{\text{blast}})}\frac{\sqrt{\left(u_c(t_{\text{blast}}) - \frac{f_c}{k_c}\right)^2\omega_d^2 + \left(\dot{u}_c(t_{\text{blast}}) + \left(u_c(t_{\text{blast}}) - \frac{f_c}{k_c}\right)\xi\omega_n\right)^2}}{\omega_d} + \frac{f_c}{k_c} \tag{18}$$

A dimensionless transfer function H_1 is then created to facilitate the design procedure:

$$H_1 = \frac{u_{c,\max}}{\frac{F_m}{k_c}} = \frac{u_{c,\max}}{u_{\text{st}}} \tag{19}$$

where $u_{\text{st}} = \frac{F_m}{k_c}$ is the static displacement from a constant peak blast force F_m.

The maximum displacement of cladding $u_{c,\ \max}$ can be obtained from Eq. 19 or from the H_1 plots as demonstrated later in Section 5 (Numerical Simulations). The maximum displacement is used to verify if $u_{c,\ \max} \le l_c$. If so, an impact rubber bumper with minimum thickness can be designed, and a second check can be conducted to ensure that $u_{c,\max} \le (l_c - l_r)$. Otherwise, the impact rubber needs to be carefully designed under Step 3.

4.3. Step 3: Parameters of impact rubber

An impact rubber of length l_r (Fig. 3(a)) is used to prevent the cladding system from colliding with the structure. Step 3 consists of sizing this rubber bumper. The design process starts with a second transfer function H_2

$$H_2 = \frac{I_{\text{structure}}}{I_{\text{blast}}} = \frac{m_c\dot{u}_{\text{rubber}}}{\frac{1}{2}F_m t_{\text{blast}}} \tag{20}$$

where $\dot{u}_{\text{rubber}}$ is the solution of the time derivative of Eq. 18 for $t = t_{\text{rubber}}$, which represents the time of impact with the impact bumper, I_{blast} is the impulse of the initial blast and $I_{\text{structure}}$ is the momentum of the cladding when it hits the rubber. The impact velocity of the cladding can be calculated using Eq. 18, which in turn will be used calculating the maximum deformation of the rubber.

To obtain the analytical solution of maximum rubber deformation, the rubber model is represented as a linear stiffness element to provide a more convenient mathematical form [2]. The mass of the rubber bumper is neglected, and the bumper will only provide additional resistant force when impacted by the cladding panel. Note that although a linear stiffness element cannot dissipate energy during a full cycle of harmonic motion, it can still be used to represent the rubber dynamics since only the gap-closing phase is considered. To do so, the hysteresis of the impact rubber (Fig. 5) can be compared to the hysteresis of a linear stiffness element in the approaching phase. The impact rubber is approximated using

$$F_r = k_{\text{eq}}u_r \tag{21}$$

where F_r is the damping force, k_{eq} is the linear stiffness coefficient, and u_r is the deformation of the impact rubber. Assuming a periodic excitation, the response of the equivalent system is written:

$$u_r(t) = \bar{u}_r\sin(\omega t) \tag{22}$$

where $\bar{u}_r$ is the amplitude of periodic excitation. To avoid the case of exceeding the ultimate compression capacity $u_{r,\ \text{ult}}$ in Fig. 5, $\bar{u}_r$ is assumed to be half of the thickness of impact rubber due to $u_{r,\text{ult}} = 80\%l_r$ reported in Reference [49]. Eq. 21 becomes

$$F_r = k_{\text{eq}}\bar{u}_r\sin(\omega t) \tag{23}$$

The energy dissipation of the impact rubber W_r for this quarter cycle response using this equivalent energy dissipation representation is expressed

$$W_r = \int_0^{\bar{u}_r} k_{\text{eq}}u_r\,du_r = \frac{1}{2}k_{\text{eq}}\bar{u}_r^2 \tag{24}$$

In addition, the energy dissipation of the impact rubber can be taken as the area under the gap-closing phase curve. From Eq. 3, F_r^A represents the impact force when cladding is in the gap-closing phase, and F_r^R represents the force in restitution phase. To simplify the integration, an integer value is used for the exponent. Neglecting the post yield phase of impact rubber, the energy dissipation in the approaching phase can be computed using Polycarpou's dynamic model for rubber (Eq. 3):

$$W_r = \int_0^{\bar{u}_r} F_r^A\,du_c = \int_0^{\bar{u}_r} k_r u_r^{2.65}\,du_r = \frac{1}{3.65}k_r\bar{u}_r^{3.65} \tag{25}$$

Equating Eq. 24 and Eq. 25 gives

$$k_{\text{eq}} = \frac{2k_r\bar{u}_r^{1.65}}{3.65} \tag{26}$$

The equivalent energy dissipation concept is illustrated in Fig. 7. The red triangle area represents energy dissipation from the linear stiffness element and the gray shaded area represents the energy dissipation from the impact rubber, where both areas are equal. Eq. 10(b) is modified to include the dynamics of the impact rubber using the equivalent stiffness concept:

$$m\ddot{u}_c(t) + c\dot{u}_c(t) + (k + k_{\text{eq}})u_c(t) = -f_c \tag{27}$$

where $t > t_{\text{rubber}}$. The rubber deformation follows the cladding displacement from the point where $u_c = u_{c,\max}$. The analytical solution for the rubber deformation is similar to Eq. 16, but with $k_{\text{new}} = k_{\text{eq}} + k_c$, where ξ_r and ω_{dr} are the modified damping ratio and damped frequency.

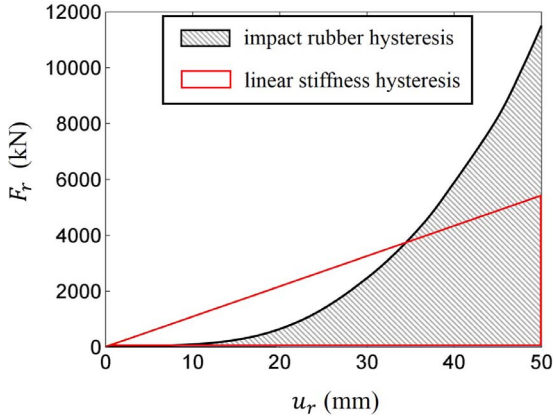

Fig. 7. Equivalent linear stiffness hysteresis.

$$u_r(t) = e^{-\xi_r \omega_{dr}(t-t_{\text{rubber}})}\left[-\frac{f_c + k_c u_c(t_{\text{rubber}})}{k_{\text{new}}}\cos\omega_{\text{dr}}(t - t_{\text{rubber}})\right] + e^{-\xi_r \omega_{\text{dr}}(t-t_{\text{rubber}})}\left[\frac{\dot{u}_c(t_{\text{rubber}})k_{\text{new}} - (f_c + k_c u_c(t_{\text{rubber}}))\xi_r\omega_r}{k_{\text{new}}\omega_{\text{dr}}}\sin\omega_{\text{dr}}(t - t_{\text{rubber}})\right] + \frac{f_c + k_c u_c(t_{\text{rubber}})}{k_{\text{new}}} \quad (28)$$

where $u_c(t_{\text{rubber}}) = l_c - l_r$ is the space between the cladding element and the impact rubber. Using the analytical solution from Eq. 28 and the time of maximum deformation $u_{r,\,\max}$, a third transfer function H_3 is obtained:

$$t_2 = \frac{\tan^{-1}\left(\frac{\dot{u}_c(t_{\text{rubber}})k_{\text{new}}\sqrt{1-\xi_r^2}}{-f_c\omega_r - k_c u_c(t_{\text{rubber}})\omega_r + \xi_r k_{\text{new}}\dot{u}_c(t_{\text{rubber}})}\right)}{\omega_{\text{dr}}} + t_{\text{rubber}} \quad (29)$$

$$u_{r,\max} = e^{-\xi_r\omega_{\text{dr}}(t_2 - t_{\text{rubber}})}\frac{\sqrt{(u_c(t_{\text{rubber}})k_c + f_c)^2\omega_{\text{dr}}^2 + (\dot{u}_c(t_{\text{rubber}})k_{\text{new}} - (u_c(t_{\text{rubber}})k_c + f_c)\xi_r\omega_r)^2}}{\omega_{\text{dr}}k_{\text{new}}} + \frac{f_c + k_c u_c(t_{\text{rubber}})}{k_{\text{new}}} \quad (30)$$

$$H_3 = \frac{u_{r,\max}}{u_{\text{st}}} \quad (31)$$

where $u_{\text{st}} = \frac{F_m}{k_c}$ is the static deformation. Transfer function H_3 provides the deformation of the impact rubber based on the design parameters selected under Steps 1 and 2, with the objective to obtain a rubber deformation smaller than its design thickness l_r. Otherwise, other design parameters need to be selected and the PBD procedure be iterated, as explained earlier.

5. Numerical simulations

In this section, numerical simulations are conducted to verify the proposed PBD methodology. Simulations are based on a 1:4 scale six-story three-bay structure equipped with cladding panels spanning each floor. This structure was selected due to the availability of parameters and results found in the literature [3,57], in which the authors studied an advanced passive energy-dissipating cladding connector for seismic design. Here, we used the cladding panel material consistent with [57], and replaced the connector by the proposed semi-active connection. Each cladding panel is attached to the structure using two tie back connectors and two bearing supports. The semi-active connection is installed as a replacement to tie back connectors, and only the bearing connectors are assumed to provide lateral stiffness and inherent damping between the cladding and the structure (k_c and c_c, respectively).

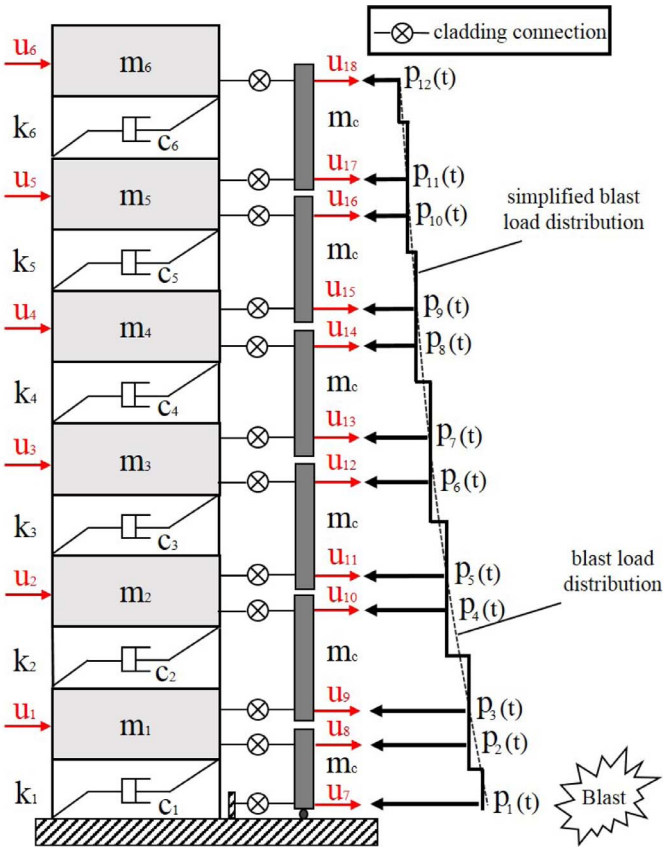

Fig. 8. Simulated structure with cladding panels.

5.1. Model assumption

5.1.1. 18DOF system

The 18DOF representation is illustrated in Fig. 8, which contains one translational DOF per floor, and two translational DOF per connection between the cladding and structure. Each cladding panel is modeled as a rigid bar of mass m_c and has two degree of freedoms at either end connected to the structure. Again, the nonlinear response of the cladding will be considered in future work, and the assumption of a rigid bar is consistent with current approaches for conservatively calculating the base shear and cladding-to-structure load transfer for buildings under blast loading [45,46]. The first cladding element spanning between ground level and the first floor has its lower semi-active connection directly attached to the ground. Details of the cladding connections are schematized in Fig. 3(a) . The dynamic properties of the structure and cladding elements are listed in Table 1, based on the properties provided in Reference [57].

The equation of motion for the 18DOF system has the form

$$\mathbf{M\ddot{u}} + \mathbf{C\dot{u}} + \mathbf{Ku} = \mathbf{E}_p\mathbf{P} + \mathbf{E}_f\mathbf{F} \quad (32)$$

where $\mathbf{u} \in \mathbb{R}^{18\times1}$ is the displacement vector, $\mathbf{P} \in \mathbb{R}^{12\times1}$ is the blast loading input vector, $\mathbf{F} \in \mathbb{R}^{12\times1}$ is the control force vector including the friction force and rubber damping force, $\mathbf{M} \in \mathbb{R}^{18\times18}$, $\mathbf{C} \in \mathbb{R}^{18\times18}$, $\mathbf{K} \in \mathbb{R}^{18\times18}$ are the mass, damping, and stiffness matrices, respectively, and $\mathbf{E}_p \in \mathbb{R}^{18\times12}$, and $\mathbf{E}_f \in \mathbb{R}^{18\times12}$ are the blast loading and control input location matrices, respectively.

The state-space representation of Eq. (32) is given by

Table 1
Dynamic properties of cladding structure [57].

floor	mass (kg)	stiffness (kN/m)	damping (kN·s/m)	cladding mass (kg)
6	3175	3000	16.32	450
5	3175	3000	16.32	450
4	3175	3000	16.32	450
3	3175	3000	16.32	450
2	3175	3000	16.32	450
1	3175	3000	16.32	450

Table 2
Comparison of modal properties.

mode	reported [57] (Hz)	model (Hz)	difference (%)	model Γ (%)
first	1.17	1.17	0.00	86.96
second	3.88	3.47	-10.57	8.91

$$\dot{\mathbf{U}} = \mathbf{A}\mathbf{U} + \mathbf{B}_p\mathbf{P} + \mathbf{B}_f\mathbf{F} \tag{33}$$

where $\mathbf{U} = [\mathbf{u} \quad \dot{\mathbf{u}}]^T \in \mathbb{R}^{36\times 1}$ is state vector and

$$\mathbf{A} = \begin{bmatrix} \mathbf{0} & \mathbf{I} \\ -\mathbf{M}^{-1}\mathbf{K} & -\mathbf{M}^{-1}\mathbf{C} \end{bmatrix}_{36\times 36} \quad \mathbf{B}_p = \begin{bmatrix} \mathbf{0} \\ \mathbf{M}^{-1}\mathbf{E}_p \end{bmatrix}_{36\times 12} \quad \mathbf{B}_f = \begin{bmatrix} \mathbf{0} \\ \mathbf{M}^{-1}\mathbf{E}_f \end{bmatrix}_{36\times 12}$$

where $\mathbf{I}$ is an 18×18 identity matrix.

Table 2 compares modal parameters between the values reported in [57] and the ones from the 18DOF model. The first mode of the model matches the first mode of the six-story building, and the modal participation factor Γ shows that the first mode largely dominates the response of the 18DOF representation. Two design blast loads are considered for this study. The first is based on a 500-kg mass of TNT (approximate explosive mass in a closed van delivery method [52]) at a standoff distance of 25 m. This load will be used in Sections 5.2 and 5.3 to compare the proposed analytical solution with the numerical results and demonstrate the PBD procedure. A smaller charge weight of 100-kg of TNT (approximate explosive mass in a compact car trunk delivery method [52]) at the same 25-m standoff will be introduced in Section 5.4 to evaluate the performance of the proposed model and procedure for a more moderate blast load. There is a greater potential for nonlinear cladding response due to the 500-kg charge than the 100-kg charge, and comparing their effects will evaluate the effectiveness of the proposed connections for a range of blast reaction magnitudes.

The amplitude of blast load F_m for both charge weights are calculated using Eq. 7 based on the maximum blast pressure $\sigma_{\max}$ and a total cladding panel area A_c of 3.33 m^2 at each floor. Parameter values of the 500-kg design blast load for each nodes are listed in Table 3 (values for the 100-kg charge will be provided later in Section 5.4). The resulting values $\sigma_{\max}$ are within a typical range σ_{cap} as discussed in Section 3.2.

Table 3
Design blast load (500-kg TNT) for 18DOF system.

node	R (m)	Z (m/kg$^{1/3}$)	$\sigma_{\max}$ (kPa)	F_m (kN)	t_{blast} (ms)
u_7	25.00	3.15	224.00	370.67	24
u_8	25.27	3.18	218.05	359.78	24
u_9	25.27	3.18	218.05	359.78	24
u_{10}	26.05	3.28	200.25	330.42	25
u_{11}	26.05	3.28	200.25	330.42	25
u_{12}	27.30	3.44	176.03	290.45	25
u_{13}	27.30	3.44	176.03	290.45	25
u_{14}	28.97	3.65	150.29	247.98	25
u_{15}	28.97	3.65	150.29	247.98	25
u_{16}	30.98	3.90	126.37	208.50	26
u_{17}	30.98	3.90	126.37	208.50	26
u_{18}	33.27	4.18	105.79	174.56	26

Table 4
Model parameters for 2DOF representation.

	parameter	value	unit
system	m_s	19,051	kg
	k_s	1029	kN/m
	c_s	56	kN·s/m
	m_c	2700	kg
blast	W	500	kg
	R	25	m
	Z	2.5	m/kg$^{1/3}$
	$\sigma_{\max}$	218	kPa
	F_m	3419	kN
	t_{blast}	24	ms

The pressure is taken as a constant between two half floors, resulting in the blast load equal for adjacent connections ($p_4 = p_5$ in Fig. 8, for instance).

5.1.2. 2DOF system

The six story structure is also modeled as 2DOF system by lumping the six structural mass elements m_s into a single mass (1DOF) and the six cladding mass elements m_c into a single cladding element to obtain a representation similar to the one schematized in Fig. 3(b). A structural damping ratio of 2% is assumed. A simplified triangular blast load is used for the simulations ($p(t)$) using blast load parameters calculated following the approach described in Section 4.1.1. The peak design blast load F_m used in 2DOF system is summation of blast peak load in 18DOF system. Note that this 2DOF system assumption is only used for verifying the SDOF approximation and it does not necessarily represent the dynamic of 18DOF system. The resulting parameters used for the numerical simulation are listed in Table 4. Remark that a different value for k_c than the one used in Reference [57] to obtain a more compliant connection to improve energy mitigation.

5.2. Verification of the SDOF approximation

Before conducting simulations of the 18DOF system, the PBD methodology is first verified for the 2DOF representation of the building to demonstrate the assumption that cladding can be designed based on an SDOF approximation. The validity of the assumption is investigated through the comparison of transfer function plots obtained from the PBD procedure and from numerical simulations. In what follows, the PBD transfer functions H_i (i = 1, 2, 3) are compared against the transfer functions of the 2DOF H_i^* obtained numerically, using a performance metric $\widetilde{H}_i$:

$$\widetilde{H}_i = \frac{H_i - H_i^*}{H_i^*} \quad \text{for i} = 1,\ 2,\ 3 \tag{34}$$

First, H_1 and H_1^* transfer functions are plotted as functions of the blast duration ratio t_{blast}/T_n for different friction capacity ratios f_c/F_m in Fig. 9(a), over the range 0.1% to 3.0%. The performance metric $\widetilde{H}_1$ is plotted in Fig. 9(b). The error in H_1 is larger for small ratios t_{blast}/T_n, and converges to 0 with increasing t_{blast}/T_n. The magnitude of the error increases with increasing friction ratio. Generally, the error is positive, which results in an over-estimation of the cladding displacement. The error is negative for a zero friction ratio ($f_c/F_m = 0\%$), because the blast energy will be transmitted to the structure (no dissipation) and the model will underestimate cladding displacement due to the unmodeled displacement of the structure.

Second, transfer function H_2 is verified through the investigation of its fitting performance index $\widetilde{H}_2$ over different values of relative rubber thickness $(l_c - l_r)/u_{st}$. Plots are shown in Figs. 10 and 11 for the ratio range 1% to 4%, which represents a large range of spacing $l_c - l_r$ as u_{st} is relatively large under blast load. A null value for H_2 signifies that the cladding does not collide with the structure. The error $\widetilde{H}_2$ is high for H_2

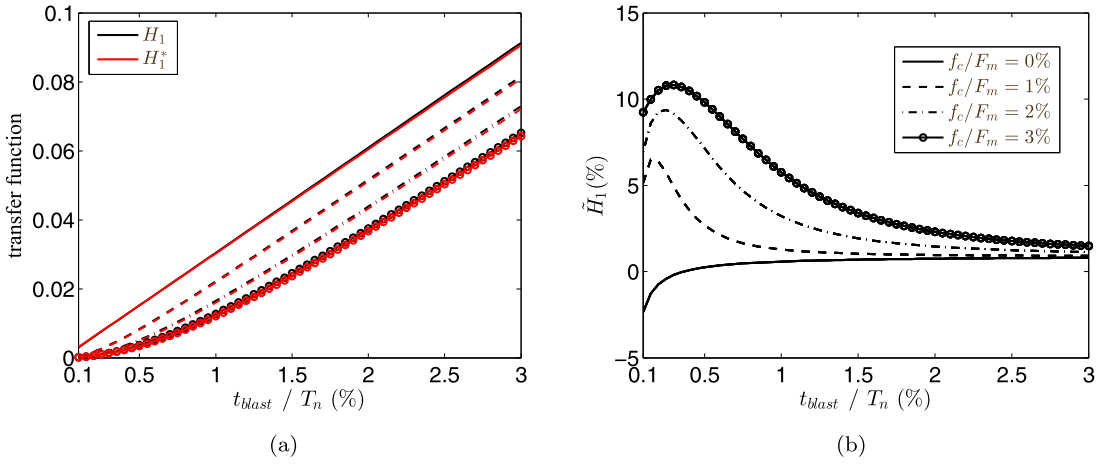

Fig. 9. H_1 function for $\xi = 2\%$: (a) H_1 and H_1^*; and (b) $\widetilde{H}_1$.

close to 0, and increases with increasing relative rubber thicknesses. The error is also higher for increasing friction ratio. In both cases, this high level of error is due to increasing nonlinearities that are not captured by the analytical solutions. However, the error is positive in all cases, which signifies that the cladding will be over-designed therefore provide additional safety. Also, the error converges to zero with increasing blast duration ratio.

Third, the H_3 function is plotted under different friction capacity ratios f_c/F_m, relative rubber thickness ratios $(l_c - l_r)/u_{st}$ and impact rubber stiffness ratios k_c/k_r in Figs. 12, 13, 14, 15. The error $\widetilde{H}_3$ is high when rubber has smaller deformations (H_3 close to 0). As t_{blast}/T_n increases, the error $\widetilde{H}_3$ quickly decreases to reach a negative value for a higher relative rubber stiffness or lower ratio k_c/k_r.

5.3. Demonstration of PBD procedure

In this section, the proposed PBD procedure is demonstrated using the six-story structure shown in Fig. 8. Recall that, similar to Section 5.2, the 500-kg charge size is used to make this comparison. The dynamic parameters of the cladding system and impact rubber, at each floor, are designed based on the PBD transfer function results H_i (i = 1, 2, 3) obtained in the previous section for an SDOF system.

Step 1: Performance Criteria

The design blast load parameters F_m and t_{blast} for each node are taken from Table 3. The spacing l_c at each floor is set to 0.4 m for the preliminary design, based on the minimum requirements reviewed in Section 4.1.2.

Step 2: Dynamic Parameters of Cladding System

The mass of each cladding panel m_c is taken as fixed, as provided in Reference [57]. Using the H_1 plot (Fig. 9(a))with the assumption of a cladding damping ratio ξ = 2%, a blast duration ratio t_{blast}/T_n = 3% with a friction capacity ratio f_c/F_m = 1% yields H_1 = 0.081. This H_1 value is used to compute $u_{c,\ \max}$ at each floor using Eq. 19. Table 5 lists the results for each node, as well as k_c and c_c to obtain t_{blast}/T_n = 3% and ξ = 2%. With these design parameters, all of the nodes exceed the allowable deformation of 0.4 m, necessitating design step 3 for appropriate sizing of the impact rubber.

Step 3: Parameters of Impact Rubber

For simplicity, both the cladding-structure spacing l_c = 0.4 m and the rubber thickness l_r are assumed constant throughout the height of the structure. The design of l_r is based on the blast load at the first floor, which represents the worst case scenario. An initial rubber thickness is selected taking $(l_c - l_r)/u_{st}$ = 1% and yielding l_r = 0.12m. The ultimate compression capacity is $u_{r,\text{ult}} = 0.8l_r$ = 0.096m. The value H_2 = 0.96 is obtained from the H_2 plot (Fig. 10(a)) using the design parameters from Step 2 (t_{blast}/T_n = 3%, f_c/F_m = 1%), which results in $u_{c,\max}$ = 2.21m. This value is much higher than the cladding-structure spacing l_c. Therefore, H_3 must be obtained such that $H_3 \le u_{r,\text{ult}}/u_{st}$ = 0.053. Using H_3 from Fig. 12(a), a value of k_c/k_r = 0.001% would satisfy this requirement, with H_3 = 0.0025. The resulting maximum rubber deflection is $u_{r,\max}$ = 0.068 m. Since the maximum deformation of rubber $u_{r,\ \max}$ is smaller than the rubber's design thickness l_r, the design is completed. A detailed design of the impact rubbers can be conducted using Eq. 4 with rubber properties found in Reference [49].

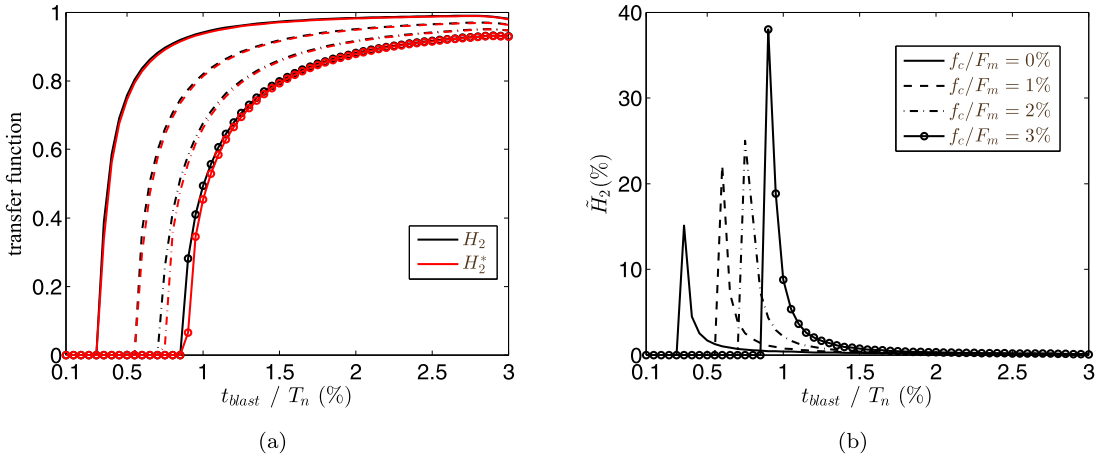

Fig. 10. H_2 function for ξ = 2% and $(l_c - l_r)/u_{st}$ = 1% : (a) H_2 and H_2^*; and (b) $\widetilde{H}_2$.

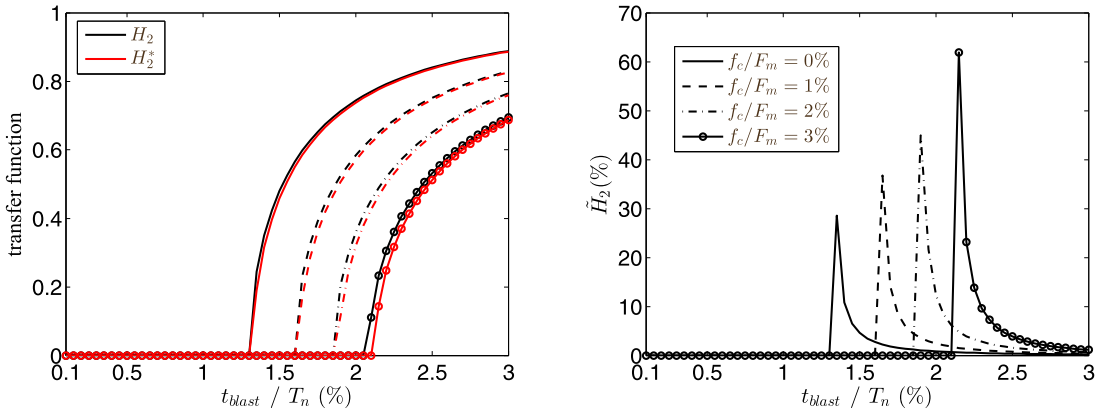

Fig. 11. H_2 function for $\xi = 2\%$ and $(l_c - l_r)/u_{st} = 4\%$: (a) H_2 and H_2^*; and (b) $\widetilde{H}_2$.

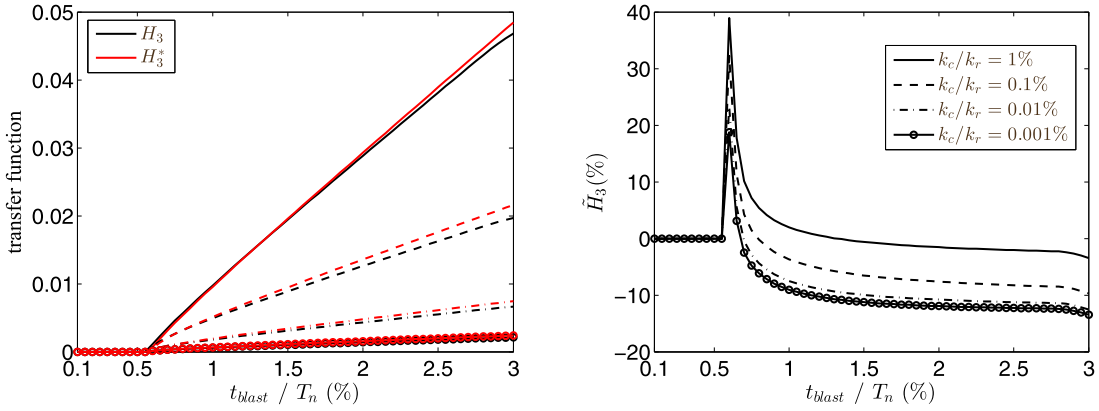

Fig. 12. H_3 function for $\xi = 2\%$, $f_c/F_m = 1\%$, and $(l_c - l_r)/u_{st} = 1\%$: (a) H_3 and H_3^*; and (b) $\widetilde{H}_3$.

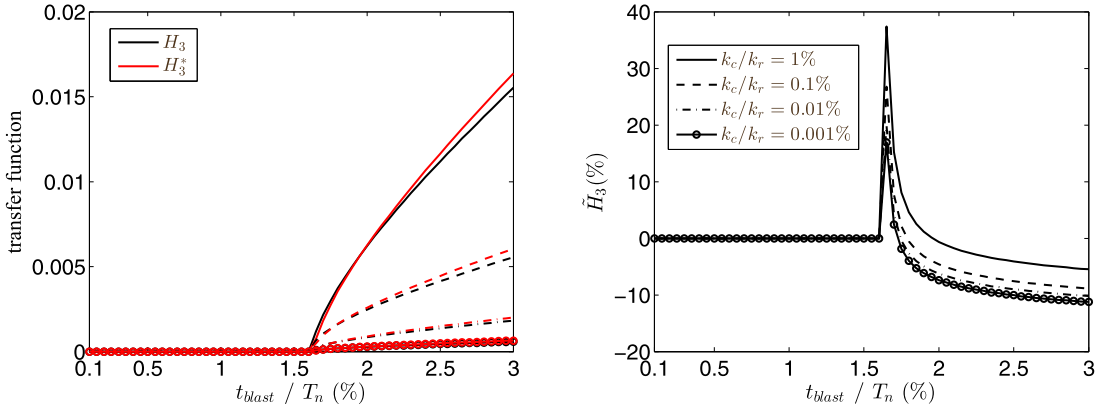

Fig. 13. H_3 function for $\xi = 2\%$, $f_c/F_m = 1\%$, and $(l_c - l_r)/u_{st} = 4\%$: (a) H_3 and H_3^*; and (b) $\widetilde{H}_3$.

5.4. Simulation results

The 18DOF model is first verified under a design blast excitation of a 500-kg charge. The discrete form of a Duhamel integral is used to numerically simulate Eq. (33) [2]:

$$\mathbf{U}(t+1) = e^{\mathbf{A}\Delta_t}\mathbf{U}(t) + \mathbf{A}^{-1}\left(e^{\mathbf{A}\Delta_t} - \mathbf{I}\right)[\mathbf{B}_f\mathbf{F}(t) + \mathbf{B}_p\mathbf{P}(t)] \tag{35}$$

where Δ_t is the time interval used in the simulation, taken as 0.0001s. Fig. 16 is a plot of the maximum cladding and rubber displacement results. The maximum rubber and cladding deformations at each node are compared with design values l_c=0.4m and l_r=0.12m. Maximum deformation of rubber reduce from first floor (node 8) to top floor (node 18) caused from decreasing peak blast load. All deformations are smaller than design values, demonstrating that the proposed PBD procedure from an SDOF system provides an adequate design methodology for an MDOF system.

The performance of proposed connection (“controlled” case) at mitigating inter-story drift and acceleration is also evaluated versus a

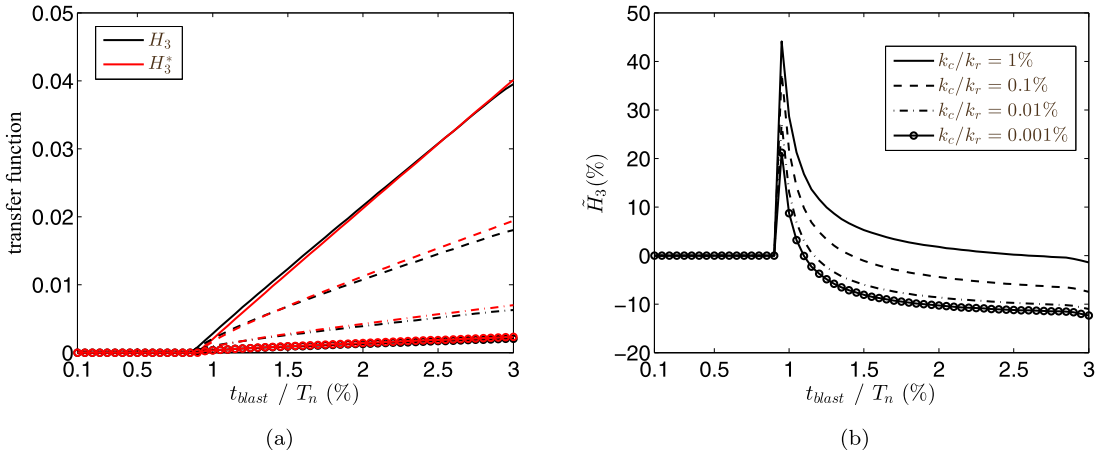

Fig. 14. H_3 function for $\xi = 2\%$, $f_c/F_m = 3\%$, and $(l_c - l_r)/u_{st} = 1\%$: (a) H_3 and H_3^*; and (b) $\widetilde{H}_3$.

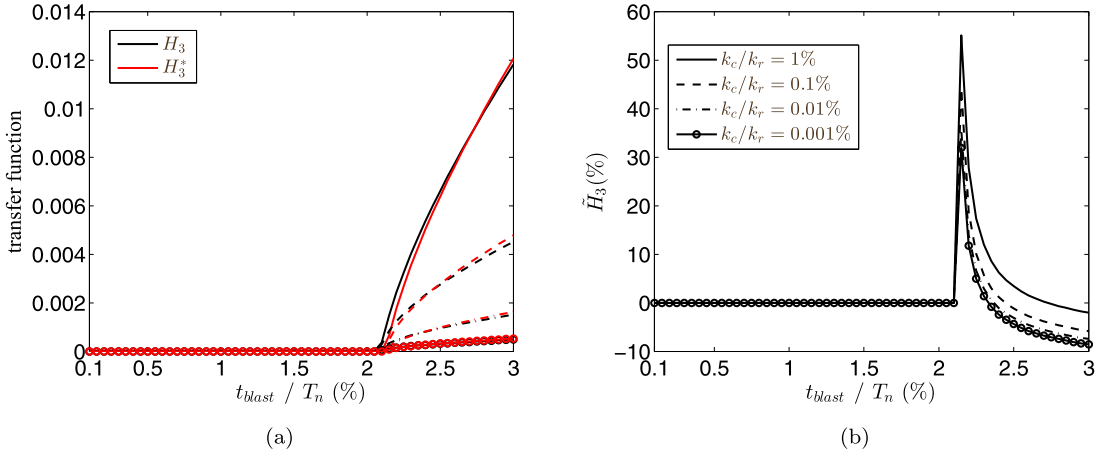

Fig. 15. H_3 function for $\xi = 2\%$, $f_c/F_m = 3\%$, and $(l_c - l_r)/u_{st} = 4\%$: (a) H_3 and H_3^*; and (b) $\widetilde{H}_3$.

Table 5
Cladding connection design parameters from Step 2.

node	m_c (kg)	T_n (s)	k_c (kN/m)	c_c (kN·s/m)	f_c (kN)	u_{st} (m)	$u_{c,\,max}$ (m)
u_7	225	0.76	15.11	7.38×10^{-2}	3.71	27.27	2.21
u_8	225	0.76	15.11	7.38×10^{-2}	3.60	26.62	2.16
u_9	225	0.76	15.11	7.38×10^{-2}	3.60	26.62	2.16
u_{10}	225	0.76	15.11	7.38×10^{-2}	3.30	24.85	2.01
u_{11}	225	0.76	15.11	7.38×10^{-2}	3.30	24.85	2.01
u_{12}	225	0.76	15.11	7.38×10^{-2}	2.90	22.40	1.81
u_{13}	225	0.76	15.11	7.38×10^{-2}	2.90	22.40	1.81
u_{14}	225	0.8	15.11	7.38×10^{-2}	2.48	19.74	1.60
u_{15}	225	0.8	13.88	7.07×10^{-2}	2.48	19.74	1.60
u_{16}	225	0.8	13.88	7.07×10^{-2}	2.09	17.21	1.40
u_{17}	225	0.8	13.88	7.07×10^{-2}	2.09	17.21	1.40
u_{18}	225	0.8	13.88	7.07×10^{-2}	1.75	14.97	1.21

cladding system attached with conventional connections ("uncontrolled" case), where k_c is assumed to be infinitely stiff and no lateral stiffness is provided by the cladding [57]. A comparison of the time series inter-story displacements at the first and top floors under design blast load are plotted in Figs. 17 and 18, as well as the corresponding rubber peak deformations. Results demonstrate that proposed cladding system provides great mitigation performance under significant blast excitation. The peak deformation of the rubber impact bumpers is larger at the first impact, as expected.

To evaluate the relative effectiveness of the proposed connection under more moderate blast loads (for which nonlinear cladding response may realistically be less likely), additional simulations of the 18DOF numerical model are conducted using the blast loads due to the 100-kg charge mass of TNT. Parameter values of this excitation are calculated based on Section 4.1.1 and are listed in Table 6.

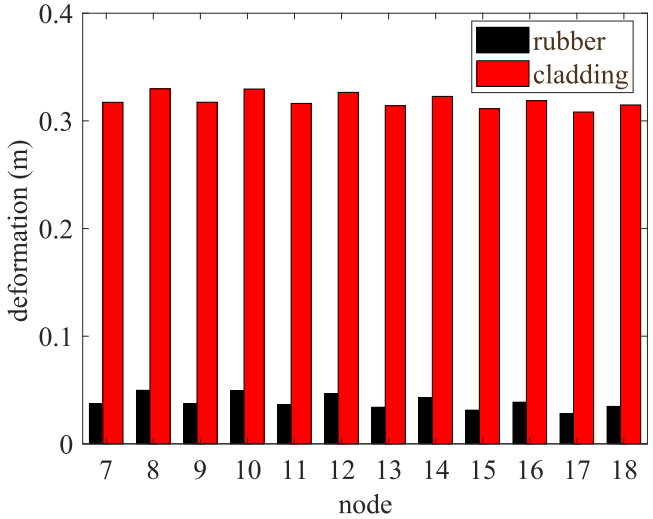

Fig. 16. Maximum deformation of cladding and rubber.

The maximum inter-story drift and acceleration reductions at each floor resulting from the controlled case under various blast excitations are compared and listed in Table 7. The cladding system under 100-kg

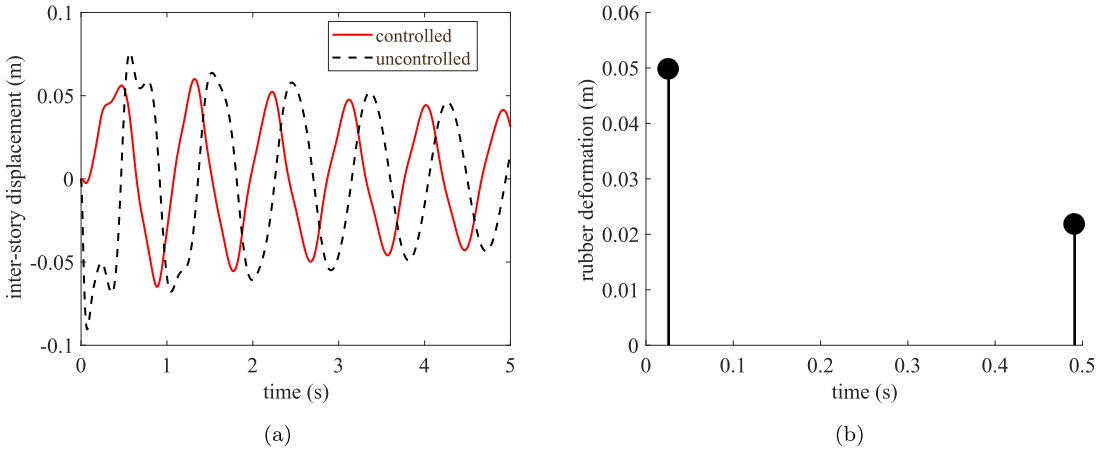

Fig. 17. (a) Comparison of displacement response at first floor; (b) peak rubber deformation at node 8 (zoom on 0.5s).

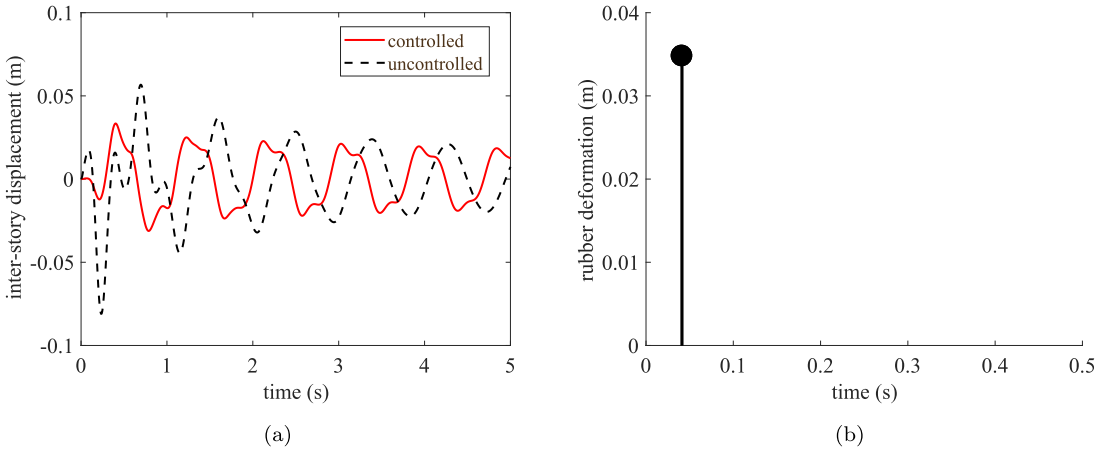

Fig. 18. (a) Comparison of displacement response at top floor; (b) peak rubber deformation at node 18 (zoom on 0.5s).

Table 6
Simulated blast load (100-kg TNT) for 18DOF system.

node	R (m)	Z (m/kg$^{1/3}$)	σ_{max} (kPa)	F_m (kN)	t_{blast} (ms)
u_7	25.00	5.39	59.49	98.16	28
u_8	25.27	5.44	58.20	96.03	28
u_9	25.27	5.44	58.20	96.03	28
u_{10}	26.05	5.61	54.67	90.21	28
u_{11}	26.05	5.61	54.67	90.21	28
u_{12}	27.30	5.88	49.75	82.09	29
u_{13}	27.30	5.88	49.75	82.09	29
u_{14}	28.97	6.23	44.35	73.18	29
u_{15}	28.97	6.23	44.35	73.18	29
u_{16}	30.98	6.66	39.11	64.54	30
u_{17}	30.98	6.66	39.11	64.54	30
u_{18}	33.27	7.15	34.40	56.75	30

Table 7
Maximum response reduction.

floor	500-kg TNT		100-kg TNT	
	inter-story drift (%)	acceleration (%)	inter-story drift (%)	acceleration (%)
1	28.32	90.93	30.20	89.93
2	26.91	87.19	32.83	86.43
3	31.22	88.54	45.93	88.06
4	47.27	78.42	40.65	82.64
5	58.79	84.81	43.38	85.31
6	67.67	71.68	38.93	79.80

TNT provides higher inter-story reduction values than the 500-kg case below the third floor due to lower peak blast load values. Above the third floor, the 500-kg case demonstrates better inter-story drift mitigation since no rubber-cladding collision and energy dissipation from impact rubber occur for the 100-kg case. Under both blast load scenarios, the decrease of inter-story drift reduction from the first to the third floor are caused by a reduced cladding stiffness and friction capacity (Table 5). Above the third floor, the performance increases as the peak blast load magnitude rapidly decreases with increasing diagonal standoff. Comparing the overall acceleration mitigation shows that the designed cladding system can provide significant improvement for different severities of blast excitations. The high acceleration reduction is caused by the absorption of the blast reaction at the cladding level.

6. Conclusions

Explosive materials deliver large shock-wave pressures to nearby structures and can cause significant damage in a very short duration. Typically, cladding systems for buildings are connected to the structure using connections with very high stiffness, which provide direct transfer of blast-induced reactions to the structural system. In this paper, a novel semi-active cladding connection is proposed for mitigating this high-rate load transfer. Instead of simply providing rigid lateral support for cladding, this new mechanism is an active participant in energy dissipation under blast load. A semi-active friction mechanism is used to provide a variable damping force, and an impact rubber bumper is utilized to absorb pounding energy for large connection displacements.

A performance-based procedure has been proposed for the design of this new cladding connection. It contains three steps: (1) blast load design, (2) cladding and friction device design, and (3) impact rubber design. Three dimensionless transfer functions were derived using an equivalent SDOF system. These functions allow rapid preliminary design of the cladding system and have been verified by numerical simulation of the 2DOF system. Results show that the PBD procedure offers adequate design values with positive performance metrics in most cases. It is computationally convenient and reasonably accurate to implement the design value from the SDOF system for the MDOF system. Negative error values may arise in the design of the rubber bumper for a limited range of scenarios, but this can be accommodated by recommending a slightly larger design thickness value to provide additional safety.

Furthermore, the proposed cladding connection was designed and simulated in a six story structure as an example for the proposed PBD procedure. A 18DOF system is used as a prototype, and the blast-induced performance of the structure with the proposed friction-based connections is compared with that using conventional cladding connections. Numerical simulation results show that the proposed cladding connection offers significant reductions of blast-induced story displacements and accelerations. Moreover, the simulation results show that the largest rubber deformation occurs in the first cladding impact cycle, which supports the assumptions inherent in models associated with the PBD approach. The results of this study indicate that this new semi-active cladding system shows promise for practical considerations of blast mitigation for buildings.

Acknowledgments

This material is based upon the work supported by the National Science Foundation under Grant No. 1463252 and No. 1463497. Their support is gratefully acknowledged. Any opinions, findings and conclusions or recommendations expressed in this material do not necessarily reflect the views of the National Science Foundation.

References

[1] Whittaker A, Hamburger R, Mahoney M. Performance-based engineering of buildings for extreme events. AISC-SINY Symposium on Resisting Blast and Progressive Collapse. 2003. p. 55–66.
[2] Connor J, Laflamme S. Structural motion engineering. Springer; 2014.
[3] Goodno B, Craig J, El-Gazairly L, Hsu C. Use of advanced cladding systems for passive control of building response in earthquakes. Proceedings, 10th World Conference on Earthquake Engineering, July. 1992. p. 19–24.
[4] Petrini F, Palmeri A. Performance-based design of bridge structures subjected to multiple hazards: a review. 6th International Conference on Bridge Maintenance, Safety and Management. 2012. p. 2040–7.
[5] Maneetes H, Memari A. Introduction of an innovative cladding panel system for multi-story buildings. Buildings 2014;4(3):418–36. http://dx.doi.org/10.3390/buildings4030418.
[6] Baird A, Palermo A, Pampanin S. Controlling seismic response using passive energy dissipating cladding connections. 2013 NZSEE Conference. 2013.
[7] Wu C, Huang L, Oehlers DJ. Blast testing of aluminum foam–protected reinforced concrete slabs. J Perform Constr Facil 2011;25(5):464–74. http://dx.doi.org/10.1061/(asce)cf.1943-5509.0000163.
[8] Shim C, Yun N, Yu R, Byun D. Mitigation of blast effects on protective structures by aluminum foam panels. Metals (Basel) 2012;2(4):170–7. http://dx.doi.org/10.3390/met2020170.
[9] Amadio C, Bedon C. Blast analysis of laminated glass curtain walls equipped by viscoelastic dissipative devices. Buildings 2012;2(4):359–83. http://dx.doi.org/10.3390/buildings2030359.
[10] Amadio C, Bedon C. Multiple dissipative devices for blast-resisting cable-supported glazing façades. Model Simul Eng 2013;2013:1–13. http://dx.doi.org/10.1155/2013/964910.
[11] Agrawal A, Yang J. Semiactive control strategies for buildings subject to near-field earthquakes. Proceedings of SPIE. 3988. 2000. p. 359.
[12] Yang J, Agrawal A. Semi-active hybrid control systems for nonlinear buildings against near-field earthquakes. Eng Struct 2002;24(3):271–80.
[13] He WL, Agrawal AK, Yang JN. Novel semiactive friction controller for linear structures against earthquakes. J Struct Eng 2003;129(7):941–50. http://dx.doi.org/10.1061/(asce)0733-9445(2003)129:7(941).
[14] Ubertini F. Prevention of suspension bridge flutter using multiple tuned mass dampers. Wind Struct 2010;13(3):235–56.
[15] Chae Y, Ricles JM, Sause R. Modeling of a large-scale magneto-rheological damper for seismic hazard mitigation. part i: passive mode. Earthquake Eng Struct Dyn 2012;42(5):669–85. http://dx.doi.org/10.1002/eqe.2237.
[16] Ubertini F, Comanducci G, Laflamme S. A parametric study on reliability-based tuned-mass damper design against bridge flutter. J Vib Control 2015;23(9):1518–34. http://dx.doi.org/10.1177/1077546315595304.
[17] Laflamme S, Taylor D, Maane MA, Connor JJ. Modified friction device for control of large-scale systems. Struct Control Health Monitor 2011;19(4):548–64. http://dx.doi.org/10.1002/stc.454.
[18] Cao L, Downey A, Laflamme S, Taylor D, Ricles J. Variable friction device for structural control based on duo-servo vehicle brake: modeling and experimental validation. J Sound Vib 2015;348:41–56. http://dx.doi.org/10.1016/j.jsv.2015.03.011.
[19] Cao L, Laflamme S, Taylor D, Ricles J. Simulations of a variable friction device for multihazard mitigation. J Struct Eng 2016;142(12):H4016001. http://dx.doi.org/10.1061/(asce)st.1943-541x.0001580.
[20] Vesselenyi T, Dziac S, Dziac I, Manolescu M-J. Fuzzy and neural controllers for a pneumatic actuator. Int J Comput Commun Control 2007;2(4):375. http://dx.doi.org/10.15837/ijccc.2007.4.2368.
[21] Mehmood A, Laghrouche S, Bagdouri ME. Modeling identification and simulation of pneumatic actuator for VGT system. Sens Actuators, A 2011;165(2):367–78. http://dx.doi.org/10.1016/j.sna.2010.11.006.
[22] Kannan S, Uras HM, Aktan HM. Active control of building seismic response by energy dissipation. Earthquake Eng Struct Dyn 1995;24(5):747–59. http://dx.doi.org/10.1002/eqe.4290240510.
[23] Lorenz M, Heimann B, Härtel V. A novel engine mount with semi-active dry friction damping. Shock Vib 2006;13(4–5):559–71. http://dx.doi.org/10.1155/2006/263251.
[24] Yang JN, Agrawal AK. Semi-active hybrid control systems for nonlinear buildings against near-field earthquakes. Eng Struct 2002;24(3):271–80. http://dx.doi.org/10.1016/s0141-0296(01)00094-3.
[25] Kawamoto Y, Suda Y, Inoue H, Kondo T. Electro-mechanical suspension system considering energy consumption and vehicle manoeuvre. Veh Syst Dyn 2008;46(sup1):1053–63. http://dx.doi.org/10.1080/00423110802056263.
[26] Chen C, Chen G. Shake table tests of a quarter-scale three-storey building model with piezoelectric friction dampers. Struct Control Health Monit 2004;11(4):239–57. http://dx.doi.org/10.1002/stc.41.
[27] Lu L-Y, Lin G-L. A theoretical study on piezoelectric smart isolation system for seismic protection of equipment in near-fault areas. J Intell Mater Syst Struct 2008;20(2):217–32. http://dx.doi.org/10.1177/1045389x08091120.
[28] Durmaz O, Clark WW, Bennett DS, Paine JS, Samuelson MN. Experimental and analytical studies of a novel semi-active piezoelectric coulomb damper. SPIE's 9th Annual International Symposium on Smart Structures and Materials. International Society for Optics and Photonics; 2002. p. 258–73.
[29] Xu YL, Ng CL. Seismic protection of a building complex using variable friction damper: experimental investigation. J Eng Mech 2008;134(8):637–49. http://dx.doi.org/10.1061/(asce)0733-9399(2008)134:8(637).
[30] Narasimhan S, Nagarajaiah S. Smart base isolated buildings with variable friction systems:h∞ controller and SAIVF device. Earthquake Eng Struct Dyn 2006;35(8):921–42. http://dx.doi.org/10.1002/eqe.559.
[31] Pardo-Varela J, de la Llera JC. A semi-active piezoelectric friction damper. Earthquake Eng Struct Dyn 2014;44(3):333–54. http://dx.doi.org/10.1002/eqe.2469.
[32] Downey A, Cao L, Laflamme S, Taylor D, Ricles J. High capacity variable friction damper based on band brake technology. Eng Struct 2016;113:287–98. http://dx.doi.org/10.1016/j.engstruct.2016.01.035.
[33] Karagiozova D, Langdon G, Nurick G. Blast attenuation in cymat foam core sacrificial claddings. Int J Mech Sci 2010;52(5):758–76. http://dx.doi.org/10.1016/j.ijmecsci.2010.02.002.
[34] Olmati P, Petrini F, Gkoumas K. Fragility analysis for the performance-based design of cladding wall panels subjected to blast load. Eng Struct 2014;78:112–20. http://dx.doi.org/10.1016/j.engstruct.2014.06.004.
[35] Wu C, Sheikh H. A finite element modelling to investigate the mitigation of blast effects on reinforced concrete panel using foam cladding. Int J Impact Eng 2013;55:24–33. http://dx.doi.org/10.1016/j.ijimpeng.2012.11.006.
[36] Linkutė L, Juocevičius V, Vaidogas ER. A probabilistic design of sacrificial cladding for a blast wall using limited statistical information on blast loading. Mechanika 2013;19(1). http://dx.doi.org/10.5755/j01.mech.19.1.3621.
[37] Ngo T, Mendis P, Gupta A, Ramsay J. Blast loading and blast effects on structures–an overview. Electronic J Struct Eng 2007;7:76–91.
[38] Li QM, Meng H. Pressure-impulse diagram for blast loads based on dimensional analysis and single-degree-of-freedom model. J Eng Mech 2002;128(1):87–92. http://dx.doi.org/10.1061/(asce)0733-9399(2002)128:1(87).
[39] Larcher M. Pressure-time functions for the description of air blast waves. JRC Technical Note 2008(46829).
[40] The design of concrete structure to resist explosions and weapon effects. Technical Manual TM 5–1300, US Department of the Army, Navy and Air Force, Washington DC 1990.
[41] Hinman E, Engineers PHC. Blast safety of the building envelope. Whole Building Design Guide,2011 2011.
[42] Ye ZQ, Ma GW. Effects of foam claddings for structure protection against blast loads. J Eng Mech 2007;133(1):41–7. http://dx.doi.org/10.1061/(asce)0733-9399(2007)133:1(41).
[43] Li B, Pan T-C, Nair A. A case study of the effect of cladding panels on the response of reinforced concrete frames subjected to distant blast loadings. Nucl Eng Des 2009;239(3):455–69. http://dx.doi.org/10.1016/j.nucengdes.2008.12.003.

[44] Zhao H, Yu H, Yuan Y, Zhu H. Blast mitigation effect of the foamed cement-base sacrificial cladding for tunnel structures. Constr Build Mater 2015;94:710–8. http://dx.doi.org/10.1016/j.conbuildmat.2015.07.076.
[45] Ewing C, Guillin C, Dhakal R, Chase J. Spectral analysis of semi-actively controlled structures subjected to blast loading. Struct Eng Mech 2009;33.
[46] Zhang R, Phillips BM. Performance and protection of base-isolated structures under blast loading. J Eng Mech 2016;142(1):04015063. http://dx.doi.org/10.1061/(asce)em.1943-7889.0000974.
[47] Anagnostopoulos SA. Pounding of buildings in series during earthquakes. Earthquake Eng Struct Dyn 1988;16(3):443–56. http://dx.doi.org/10.1002/eqe.4290160311.
[48] Davis RO. Pounding of buildings modelled by an impact oscillator. Earthquake Eng Struct Dyn 1992;21(3):253–74. http://dx.doi.org/10.1002/eqe.4290210305.
[49] Polycarpou PC, Komodromos P, Polycarpou AC. A nonlinear impact model for simulating the use of rubber shock absorbers for mitigating the effects of structural pounding during earthquakes. Earthquake Eng Struct Dyn 2012;42(1):81–100. http://dx.doi.org/10.1002/eqe.2194.
[50] Komodromos P, Polycarpou PC, Papaloizou L, Phocas MC. Response of seismically isolated buildings considering poundings. Earthquake Eng Struct Dyn 2007;36(12):1605–22. http://dx.doi.org/10.1002/eqe.692.
[51] Muthukumar S, DesRoches R. A hertz contact model with non-linear damping for pounding simulation. Earthquake Eng Struct Dyn 2006;35(7):811–28. http://dx.doi.org/10.1002/eqe.557.
[52] Draganić H, Sigmund V. Blast loading on structures. Tehnicki Vjesnik/Technical Gazette 2012;19(3):643–52.
[53] Dusenberry DO. Handbook for blast-resistant design of buildings. Wiley Online Library; 2010.
[54] Blast protection of building. American Society of Civil Engineers-Structural Engineering Institute (ASCE/SEI) 59-11, Reston, VA, 2011 2011.
[55] Mills C. The design of concrete structure to resist explosions and weapon effects. Proceedings of the 1st Int. Conference on Concrete for Hazard Protections. 1987. p. 61–73.
[56] Lam N, Mendis P, Ngo T. Response spectrum solutions for blast loading. Electron J Struct Eng 2004;4:28–44.
[57] Pinelli J-P, Craig JI, Goodno BJ. Energy-based seismic design of ductile cladding systems. J Struct Eng 1995;121(3):567–78. http://dx.doi.org/10.1061/(asce)0733-9445(1995)121:3(567).
[58] Lstiburek J. Moisture control handbook: principles and practices for residential and small commercial buildings. John Wiley & Sons; 1996.